Science AAAS

The Global Magnetic Field of Mercury from MESSENGER Orbital Observations

Brian J. Anderson *et al.*

Science **333**, 1859 (2011);
DOI: 10.1126/science.1211001

when the surface was below the sublimation temperature (that is, at night) may have produced volatile-rich deposits when magmatic gases or fumarolic minerals condensed onto the cold surroundings. These materials could then have been sequestered through burial by extensive thicknesses of pyroclastic deposits or lava. Subsequent impact cratering could have exhumed these materials to the shallow subsurface, followed by formation of depressions by scarp retreat as the volatile component sublimated.

To estimate the rate at which hollows may be forming, we used shadow-length measurements to determine the average depth of the hollows on the floor of the Raditladi basin (Fig. 1C). This value (44 m), combined with the age of the basin as constrained by the crater size-frequency distribution [10^9 years (*27*)] yields an erosion rate of 0.04 μm/year, or 1 cm in 200,000 years, under the assumption that erosion proceeds only downwards. In many areas, however, the flat floors and rounded outlines suggest that the hollows are enlarged through radial growth—down to a resistant base, then laterally by scarp retreat. We determined the characteristic average radius (137 m) for isolated hollows and individual hollows that form merged groups on the floor of Raditladi. Under strictly radial growth, the erosion rate is 0.14 μm/year, or 1 cm in 70,000 years. For comparison, estimates for the rate of scarp retreat in the martian "Swiss-cheese" terrain are ~1 m per Earth year (*22*), and the rate of abrasion of kilogram-sized lunar rocks by micrometeoroid bombardment is ~1 cm per 10^7 years (*28*). Although the uncertainties in the formation rate are large, the existence on Mercury of a process modifying the terrain faster than lunar micrometeoroid erosion but more slowly than martian CO_2 ice sublimation can account for why the hollows appear to be much younger than the impact structures in which they are found.

The involvement of volatiles in candidate formation mechanisms for the hollows fits with growing evidence (*16*, *17*, *26*, *29*) that Mercury's interior contains higher abundances of volatile elements than are predicted by several planetary formation models for the innermost planet (*30–32*). Mercury is a small rocky-metal world whose internal geological activity was generally thought to have ended long ago. The presence of potentially recent surface modification implies that Mercury's nonimpact geological evolution may still be ongoing.

References and Notes

1. S. E. Hawkins III *et al*., *Space Sci. Rev.* **131**, 247 (2007).
2. Mercury's surface reflectance spectrum has a positive slope from ultraviolet to near-infrared wavelengths. Spectral slopes less steep than the global average are said to be "blue," and those with greater slopes are termed "red." The reflectance in 559-nm filter images is 0.140 for the hollows on Tyagaraja's floor versus 0.057 for the Mercury global average. The normalized 559-nm reflectance was measured for the continuous ejecta of 23 rayed (Kuiperian) craters and 20 BCFDs. For the Kuiperian craters, the mean reflectance is 0.09 ± 0.01. For the BCFDs, the mean reflectance is 0.107 ± 0.018.
3. D. Dzurisin, *Geophys. Res. Lett.* **4**, 383 (1977).
4. B. Rava, B. Hapke, *Icarus* **71**, 397 (1987).
5. M. S. Robinson *et al*., *Science* **321**, 66 (2008).
6. D. T. Blewett *et al*., *Earth Planet. Sci. Lett.* **285**, 272 (2009).
7. D. T. Blewett *et al*., *Icarus* **209**, 239 (2010).
8. B. W. Denevi *et al*., *Science* **324**, 613 (2009).
9. R. G. Strom, N. J. Trask, J. E. Guest, *J. Geophys. Res.* **80**, 2478 (1975).
10. P. D. Spudis, J. E. Guest, in *Mercury*, F. Vilas, C. R. Chapman, M. S. Matthews, Eds. (Univ. of Arizona Press, Tucson, AZ, 1988), pp. 118–164.
11. M. S. Robinson, P. G. Lucey, *Science* **275**, 197 (1997).
12. J. W. Head *et al*., *Science* **321**, 69 (2008).
13. J. W. Head *et al*., *Earth Planet. Sci. Lett.* **285**, 227 (2009).
14. J. W. Head *et al*., *Science* **333**, 1853 (2011).
15. S. L. Murchie *et al*., *Science* **321**, 73 (2008).
16. L. Kerber *et al*., *Earth Planet. Sci. Lett.* **285**, 263 (2009).
17. L. Kerber *et al*., *Planet. Space Sci.,* 8 April 2011 (10.1016/j.pss.2011.03.020).
18. J. J. Gillis-Davis *et al*., *Earth Planet. Sci. Lett.* **285**, 243 (2009).
19. P. H. Schultz, M. I. Staid, C. M. Pieters, *Nature* **444**, 184 (2006).
20. Fresh (immature) materials in young crater ejecta and rays have spectral slopes that are less steep ("bluer") than the global average. However, the BCFDs have more extreme blue color (*5*, *6*).
21. The minimum depth of excavation of the central peak material is assumed to be the maximum depth of impact melting, which was estimated with methods described earlier (*33*).
22. M. C. Malin, M. A. Caplinger, S. D. Davis, *Science* **294**, 2146 (2001).
23. A. Kracher, D. W. G. Sears, *Icarus* **174**, 36 (2005).
24. M. J. Loeffler, C. A. Dukes, W. Y. Chang, L. A. McFadden, R. A. Baragiola, *Icarus* **195**, 622 (2008).
25. L. R. Nittler *et al*., *Meteorit. Planet. Sci.* **36**, 1673 (2001).
26. L. R. Nittler *et al*., *Science* **333**, 1847 (2011).
27. R. G. Strom, C. R. Chapman, W. J. Merline, S. C. Solomon, J. W. Head III, *Science* **321**, 79 (2008).
28. D. G. Ashworth, Lunar and planetary impact erosion, in *Cosmic Dust*, J. A. M. McDonnell, Ed. (Wiley, Hoboken, NJ, 1977), pp. 427–526.
29. P. N. Peplowski *et al*., *Science* **333**, 1850 (2011).
30. J. S. Lewis, *Annu. Rev. Phys. Chem.* **24**, 339 (1973).
31. B. Fegley Jr., A. G. W. Cameron, *Earth Planet. Sci. Lett.* **82**, 207 (1987).
32. W. W. Benz, W. L. Slattery, A. G. W. Cameron, *Icarus* **74**, 516 (1988).
33. C. M. Ernst *et al*., *Icarus* **209**, 210 (2010).
34. During orbital mapping, the MDIS wide-angle camera collects images through filters with central wavelengths of 430, 480, 559, 629, 749, 829, 898, and 997 nm. Red–green–blue presentation is the inverse of principal component two (iPC2)–PC1–(430-nm/629-nm ratio) (*5*, *8*).
35. F. Preusker *et al*., *Planet. Space Sci.,* 28 July 2011 (10.1016/j.pss.2011.07.005).

Acknowledgments: This work was supported by NASA through the MESSENGER project and by a Participating Scientist grant to D.T.B. M. Robinson offered helpful comments on the manuscript. We thank N. Fontanella, S. Peel, E. Zhong, P. Pashai, and E. Coman for assistance with data processing and compilation. MESSENGER data are archived with the NASA Planetary Data System.

Supporting Online Material

www.sciencemag.org/cgi/content/full/333/6051/1856/DC1
SOM Text
Fig. S1

25 July 2011; accepted 5 September 2011
10.1126/science.1211681

The Global Magnetic Field of Mercury from MESSENGER Orbital Observations

Brian J. Anderson,[1]* Catherine L. Johnson,[2,3] Haje Korth,[1] Michael E. Purucker,[4] Reka M. Winslow,[2] James A. Slavin,[5] Sean C. Solomon,[6] Ralph L. McNutt Jr.,[1] Jim M. Raines,[5] Thomas H. Zurbuchen[5]

Magnetometer data acquired by the MESSENGER spacecraft in orbit about Mercury permit the separation of internal and external magnetic field contributions. The global planetary field is represented as a southward-directed, spin-aligned, offset dipole centered on the spin axis. Positions where the cylindrical radial magnetic field component vanishes were used to map the magnetic equator and reveal an offset of 484 ± 11 kilometers northward of the geographic equator. The magnetic axis is tilted by less than 3° from the rotation axis. A magnetopause and tail-current model was defined by using 332 magnetopause crossing locations. Residuals of the net external and offset-dipole fields from observations north of 30°N yield a best-fit planetary moment of 195 ± 10 nanotesla-R_M^3, where R_M is Mercury's mean radius.

Mercury and Earth are the only terrestrial planets with global magnetic fields of internal origin, but Mercury's field is weak compared with Earth's (*1–3*). Explaining the comparatively weak field at Mercury with an Earth-like magnetic dynamo in the fluid outer core has proven challenging (*4*), and innovative theoretical solutions have been proposed (*5*, *6*) that can potentially be distinguished by the field geometry. Magnetometer observations made during Mercury flybys by the Mariner 10 (*1*) and MESSENGER (*2*, *3*) spacecraft indicate that the planet's internal field is consistent with an axially aligned dipole displaced northward by ~0.16 R_M, where R_M is Mercury's mean radius, 2440 km. However, because of limited geographical coverage afforded by the flybys, the estimated dipole and quadrupole coefficients were highly correlated (*7*, *8*) such that the solutions were not unique. Moreover, signatures of plasma pressure near the equator raised questions about the field magnitudes recorded near the equator, implying that the inferred offset could have been the

[1]The Johns Hopkins University Applied Physics Laboratory, Laurel, MD 20723, USA. [2]University of British Columbia, Vancouver, BC V6T 1Z4, Canada. [3]Planetary Science Institute, Tucson, AZ 85719, USA. [4]Goddard Space Flight Center, Greenbelt, MD 20771, USA. [5]Department of Atmospheric, Oceanic and Space Sciences, University of Michigan, Ann Arbor, MI 48109, USA. [6]Department of Terrestrial Magnetism, Carnegie Institution of Washington, Washington, DC 20015, USA.

*To whom correspondence should be addressed. E-mail: brian.anderson@jhuapl.edu

result of plasma effects (*9*). On 18 March 2011, the MESSENGER spacecraft was inserted into a near-polar orbit about Mercury with a periapsis altitude of 200 km, an inclination of 82.5°, and an apoapsis altitude of 15,300 km. Here, we show that magnetic field observations from orbit provide an unambiguous determination of the global structure of the planetary magnetic field.

MESSENGER's eccentric orbit transits the equator at about 1000 km altitude on the descending orbit node (*10*). Figure 1 shows Magnetometer data (*11*) acquired shortly after instrument turn-on for orbital commissioning on 23 March 2011. Plasma pressures are indicated by irregular depressions in field magnitude from 01:49 to 01:57 Coordinated Universal Time (UTC). Despite the magnitude variability, the field direction near the equator changed smoothly, consistent with the diamagnetic effect of plasma that reduced the local field strength but did not alter the basic field geometry. Similar depressions in field strength with steady field direction were observed across the descending node on almost every orbit and are coincident with increases in proton flux recorded by MESSENGER's Fast Imaging Plasma Spectrometer (*12*).

Plasma pressures comparable to the magnetic pressure complicate the determination of the planetary magnetic field because spherical harmonic analysis has its basis in a formalism (Laplace's equation) that requires the sampled volume to be free of electric current (*13*). These magnetic field data therefore are not amenable to direct application of spherical harmonic analysis for latitudes south of ~30°N, and the dipole and quadrupole terms, g_{10} and g_{20}, remain highly correlated in solutions using MESSENGER orbital data taken only from northern latitudes (*8*). The prevalence of plasma pressure effects implies that spherical harmonic analysis will be unable to resolve the ambiguity in the internal field structure, a situation that if unresolved would severely hamper efforts to understand the mechanisms driving Mercury's magnetic field.

To make progress separating the internal and external fields, we take advantage of the fact that, for a slowly rotating system, the planetary magnetic field governs the distributions of plasma pressure and the locations of external currents (e.g., magnetopause and tail currents) such that they are symmetric in the north-south direction about the magnetic equator (*14*, *15*). At Mercury there may be a north-south shift in the cross-tail current that depends on the sign of the sunward interplanetary magnetic field (IMF) component (*16*). This shift is relative to the magnetic equator and because the sunward IMF component changes sign typically twice each solar rotation (*15*), this effect can be assessed and generally averages out. Thus, the location of the magnetic equator can be identified from the geometry of the magnetic field without the need to correct for local plasma pressures and external currents. Knowledge of the magnetic equator informs both internal and external field descriptions. For the external field, it specifies the location of the planetary dipole, which orders the external current systems (*2*). For the internal field, it specifies the ratio between the g_{10} and g_{20} terms so that the planetary moment can be determined from data northward of 30°N.

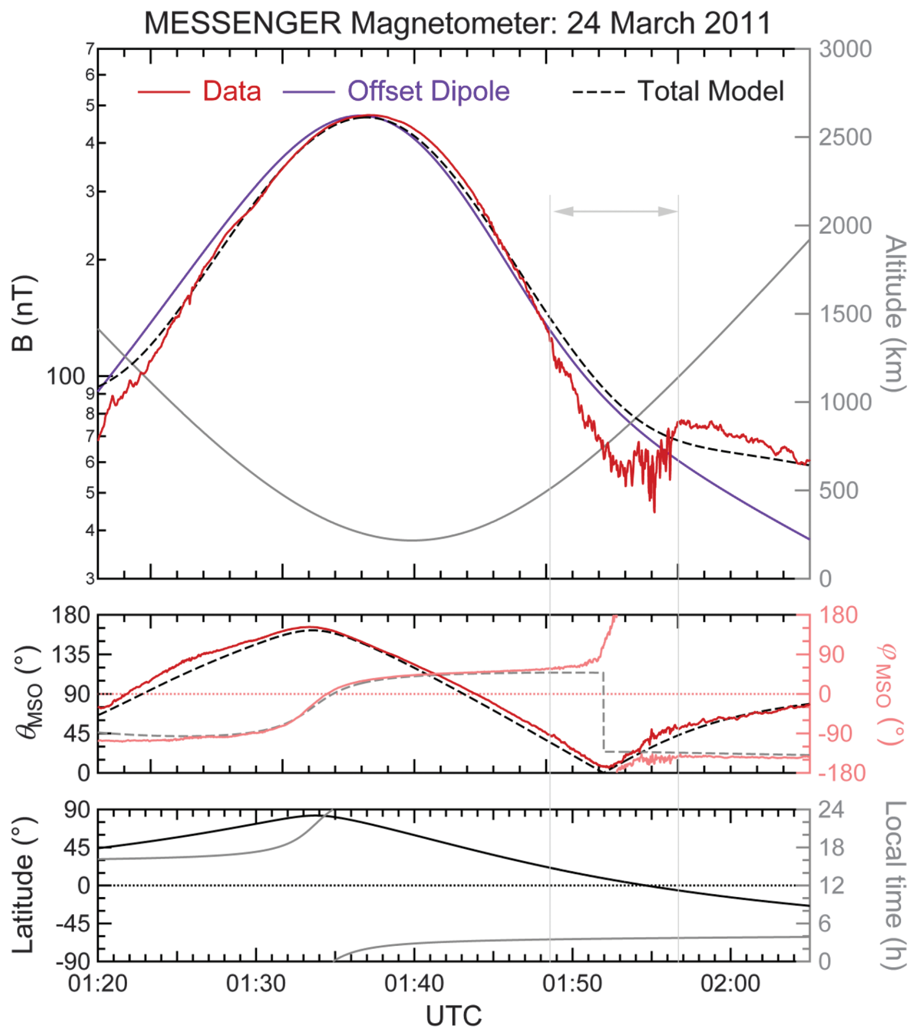

Fig. 1. MESSENGER magnetic field data for 24 March 2011 in MSO coordinates, for which *X* is sunward, *Z* is northward, and *Y* is duskward. (**Top**) The field magnitude and spacecraft altitude; (**middle**) magnetic field MSO polar angle, θ_{MSO}, and azimuth angle, φ_{MSO}; and (**bottom**) spacecraft latitude and local time. Vertical lines delimit the times of depressed magnetic field intensities near the equator. Magnetic field observations are shown in red; offset dipole field magnitude is shown in purple; the total field model (internal and external fields) magnitude and θ_{MSO} are shown in dashed black lines; and total field model φ_{MSO} is plotted as a dashed gray line.

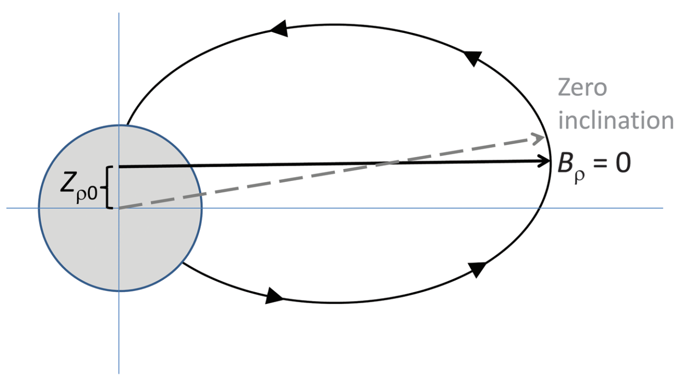

Fig. 2. Identification of magnetic equator from the zero crossing of the cyclindrical radial component of the magnetic field. For a dipole approximately aligned with the planet's spin axis, the north-south position of the $B_\rho = 0$ point coincides with the magnetic equator. For a case with a large axial offset, the point of zero inclination will overestimate the displacement relative to that given by the location of $B_\rho = 0$.

We consider the magnetic field (**B**) in cylindrical Mercury solar orbital (MSO) coordinates $(\rho, \varphi, Z)_{MSO}$, where Z_{MSO} is positive northward, φ_{MSO} is zero at the subsolar point and increases toward dusk, and ρ_{MSO} is positive outward parallel to the equatorial plane. In this system, the magnetic equator is indicated by the locus of points where $B_\rho = 0$, and the Z_{MSO} coordinate of each point, denoted by $Z_{\rho 0}$, indicates the local offset of the magnetic equator from the geographic equator of the planet (Fig. 2). The figure also illustrates that, for an axially aligned dipole, $B_\rho = 0$ is a more reliable indicator of the magnetic equator than the point of zero inclination (where the magnetic field is parallel to the planetary surface). For each descending node pass, we selected a 1-min interval centered on the $B_\rho = 0$ crossing(s) and obtained $Z_{\rho 0}$ via linear regression between B_ρ and Z_{MSO} using 1-s averaged data. The intercept yields the $Z_{\rho 0}$ estimate for that pass (see also fig. S1). On some passes outbound on the dayside, the spacecraft crossed the magnetopause close to or before crossing the magnetic equator, and $Z_{\rho 0}$ determinations were not possible.

Determinations of $Z_{\rho 0}$ for 141 passes from 23 March to 20 June 2011 (Fig. 3) demonstrate unambiguously that Mercury's dipole is displaced north of the geographic equator by a mean distance of 484 ± 11 km (3-SE uncertainty) and a sample standard deviation of 44 km. The variation with longitude is small relative to the offset. A tilt of the dipole relative to the *Z* axis should produce a single-period sinusoid, whereas the dominant variation displays about two periods in longitude. The magnetic nightside equator may shift northward for antisunward IMF and shift southward for sunward IMF (*16*). Although data between –180° and 0° longitude are consistent with this expectation, longitudes from 45° to 135° are sampled twice, and in this range there is no clear distinction in $Z_{\rho 0}$ between sunward and antisunward IMF. Additional data will be required to distinguish the effects of local time and planetary longitude.

The dipole tilt is then given by identifying the point on each pass where the magnetic field has zero inclination relative to the surface of a sphere centered on a point offset north by 484 km relative to Mercury's center. The zero-inclination point on each pass was estimated from linear regression between the field inclination and latitude in this offset coordinate system. Fitting the zero-inclination-point departures from the magnetic equator versus longitude gives an upper limit for the tilt of 3°. The longitudinal variation, however, is not entirely consistent with a tilt.

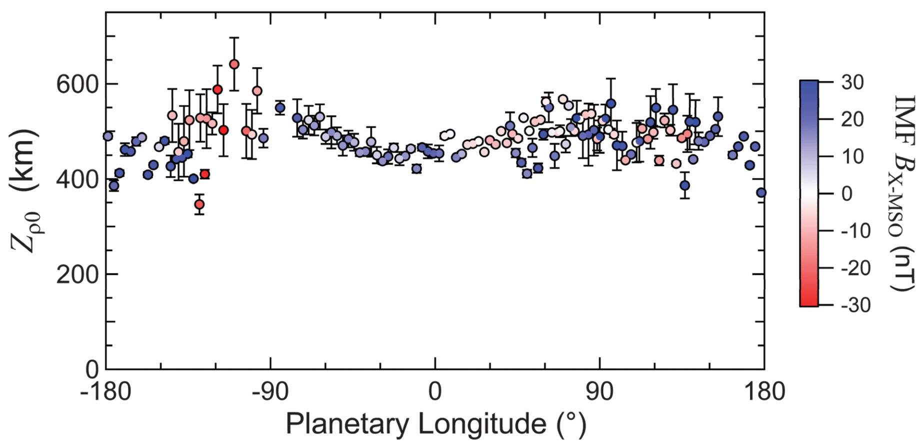

Fig. 3. Magnetic equator offset versus planetary longitude. Color coding denotes IMF $B_{X\text{-MSO}}$ averaged over a 2-hour period that combines 1 hour before the inbound bow-shock crossing and 1 hour after the outbound bow-shock crossing. Error bars are 3-SE uncertainties.

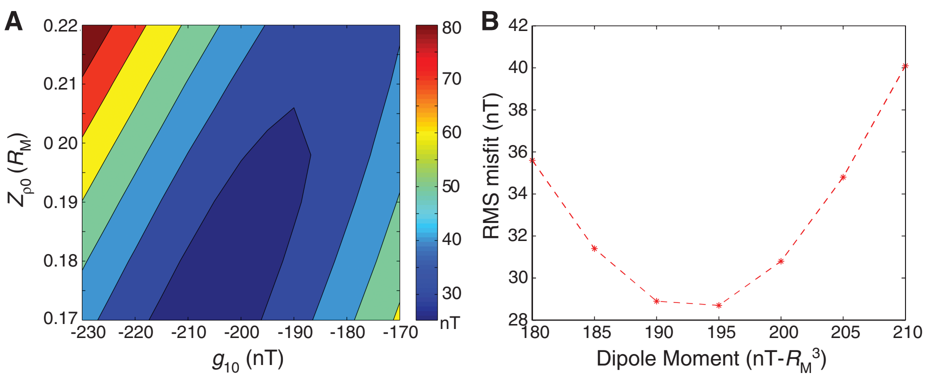

Fig. 4. Solutions for Mercury's dipole (g_{10}) obtained by applying the constraint of the quadrupole (g_{20}) corresponding to the dipole offset determined here. (**A**) Misfit versus the *Z*-axis offset (left-hand axis) and g_{10} (bottom axis). (**B**) Misfit versus dipole moment magnitude (=$|g_{10}|$ nT-R_M^3), indicating a minimum at 195 nT-R_M^3. RMS, root mean square.

Knowing the geometry of Mercury's dipole allows the magnitude of the planetary moment to be derived. This calculation requires separating the contributions from internal and external sources. The constraints on the external field model (*2*) are the position of the planetary dipole, the dipole moment, the subsolar magnetopause distance, the degree of magnetopause flaring, the distance from the planet center to the inner edge of the tail current sheet, and the tail magnetic flux. Magnetopause inbound and outbound crossings were identified for all passes in the period of study (332 crossings), and their locations were used to determine that the best-fit parabolic magnetopause is given by a subsolar distance of 1.4 R_M and minimal flaring, consistent with a closest magnetopause distance at the subsolar point. The tail current-sheet distance and magnetic flux derived from the flybys (*2*) are consistent with the orbital data, and variations in these parameters do not affect the dipole moment solutions.

Because the planetary moment determines the magnetopause current densities, we performed a parameter search revising the external model for each value of the moment and calculating the residuals of the observations north of 30°N relative to the summed internal and external fields for each moment value. The internal model was a planet-centered spherical harmonic series for which we assumed zero tilt; set the planetary moment equal to the magnitude of g_{10}; calculated g_{20} from the ratio $g_{20}/g_{10} = 2Z_{\rho 0}$ with $Z_{\rho 0}$ in R_M, using the present result for $Z_{\rho 0}$; and set all other coefficients to zero. The root mean square magnitude of the residuals (misfit) for the MESSENGER orbital data from 23 March to 20 June 2011 is shown in Fig. 4. (fig. S2 is a stereographic projection of the same residuals.) The misfit has a minimum value of 29 nT at g_{10} = –195 nT, or a corresponding moment magnitude of 195 nT-R_M^3, and grows to 35 nT for moment magnitudes of 180 and 205 nT-R_M^3 (Fig. 4B). The best estimate for g_{10} is taken to be –195 ± 10 nT (1-SD uncertainty), ~27% lower in magnitude than the centered-dipole estimate implied by the polar Mariner 10 flyby (*9*). The corresponding g_{20} value is –74 ± 4 nT. Allowing other coefficients to be nonzero and attributing all remaining residuals to the internal field gave a final g_{10} value of –202.5 nT, suggesting that the value from g_{10} in models accounting for higher-order structure will be within the estimated range. Results for the best-fit offset dipole and total model field magnitudes and direction angles are shown in Fig. 1. From MESSENGER's orbit, the external field contributes more than 20% of the total field only at lower latitudes and higher altitudes. The combined model field reproduces the orbital data north of ~30°N to within 10 to 20 nT.

The northward displacement of Mercury's magnetic dipole from the geographic equator implies a substantial north-south asymmetry in the surface field. In particular, the surface field at the north pole is a factor of 3.4 larger than at the south pole. In addition, the surface area of open magnetic flux in the southern hemisphere is about four times that in the northern hemisphere. The comparatively weak southern polar field and larger open field area in the south imply that greater particle-stimulated surface sputtering occurs in the southern polar regions, where plasmas will preferentially precipitate to the surface (*17*).

The high axisymmetry and equatorial asymmetry of Mercury's field distinguish it from the fields of Earth and other planets. Whereas large offsets of the dipole axis from the planetary center have also been inferred for both Uranus and Neptune, these planets exhibit magnetic fields that are strong relative to Earth's field and asymmetric about the rotation axis (*18*). Saturn also has a dipolar field aligned closely with and offset along the rotation axis (*18*). For Saturn the ratio g_{20}/g_{10} is about 0.072 (*18*), whereas for Mercury we find g_{20}/g_{10} ~ 0.38, reflecting a dipole offset relative to the planetary diameter that is a factor of 5 greater for Mercury. An axially aligned but differentially rotating conducting layer between a deeper internally tilted field and the exterior might account for Saturn's axially aligned field (*19*). Whether a similar mechanism could operate at Mercury is not known.

References and Notes

1. N. F. Ness, K. W. Behannon, R. P. Lepping, Y. C. Whang, *J. Geophys. Res.* **80**, 2708 (1975).
2. I. I. Alexeev *et al.*, *Icarus* **209**, 23 (2010).
3. H. Uno, C. L. Johnson, B. J. Anderson, H. Korth, S. C. Solomon, *Earth Planet. Sci. Lett.* **285**, 328 (2009).
4. S. Stanley, G. A. Glatzmaier, *Space Sci. Rev.* **152**, 617 (2010).
5. R. Vilim, S. Stanley, S. A. Hauck II, *J. Geophys. Res.* **115**, E11003 (2010).
6. A. Manglik, J. Wicht, U. R. Christensen, *Earth Planet. Sci. Lett.* **289**, 619 (2010).
7. J. E. P. Connerney, N. F. Ness, in *Mercury*, F. Vilas, C. R. Chapman, M. S. Matthews, Eds. (Univ. Arizona Press, Tucson, 1988), pp. 494–513.
8. H. Korth *et al.*, *Planet. Space Sci.* **52**, 733 (2004).
9. B. J. Anderson *et al.*, *Space Sci. Rev.* **152**, 307 (2010).
10. S. C. Solomon, R. L. McNutt Jr., R. E. Gold, D. L. Domingue, *Space Sci. Rev.* **131**, 3 (2007).
11. B. J. Anderson *et al.*, *Space Sci. Rev.* **131**, 417 (2007).
12. T. H. Zurbuchen *et al.*, *Science* **333**, 1862 (2011).
13. G. Backus, *Rev. Geophys.* **24**, 75 (1986).
14. W. Baumjohann, R. A. Treumann, *Basic Space Plasma Physics* (Imperial College Press, World Scientific Publishing, London, 1997).
15. M. G. Kivelson, C. T. Russell, *Introduction to Space Physics* (Cambridge Univ. Press, Cambridge, 1995).
16. P. Trávníček, P. Hellinger, D. Schriver, *Geophys. Res. Lett.* **34**, L05104 (2007).
17. R. Killen *et al.*, *Space Sci. Rev.* **132**, 433 (2007).
18. C. T. Russell, M. K. Dougherty, *Space Sci. Rev.* **152**, 251 (2010).
19. D. J. Stevenson, *Geophys. Astrophys. Fluid Dyn.* **21**, 113 (1982).

Acknowledgments: We thank the MESSENGER operations and engineering teams. The MESSENGER mission is supported by the NASA Discovery Program and the MESSENGER Participating Scientist Program. C.L.J. and R.M.W. acknowledge support from the Natural Sciences and Engineering Research Council of Canada.

Supporting Online Material
www.sciencemag.org/cgi/content/full/333/6051/1859/DC1
Figs. S1 and S2

11 July 2011; accepted 8 September 2011
10.1126/science.1211001

MESSENGER Observations of the Spatial Distribution of Planetary Ions Near Mercury

Thomas H. Zurbuchen,[1]* Jim M. Raines,[1] James A. Slavin,[1,2] Daniel J. Gershman,[1] Jason A. Gilbert,[1] George Gloeckler,[1] Brian J. Anderson,[3] Daniel N. Baker,[4] Haje Korth,[3] Stamatios M. Krimigis,[3,5] Menelaos Sarantos,[2,6] David Schriver,[7] Ralph L. McNutt Jr.,[3] Sean C. Solomon[8]

Global measurements by MESSENGER of the fluxes of heavy ions at Mercury, particularly sodium (Na^+) and oxygen (O^+), exhibit distinct maxima in the northern magnetic-cusp region, indicating that polar regions are important sources of Mercury's ionized exosphere, presumably through solar-wind sputtering near the poles. The observed fluxes of helium (He^+) are more evenly distributed, indicating a more uniform source such as that expected from evaporation from a helium-saturated surface. In some regions near Mercury, especially the nightside equatorial region, the Na^+ pressure can be a substantial fraction of the proton pressure.

Mercury's dipole magnetic field, particularly its small magnitude and near-alignment with the planet's rotation axis, defines the planet's interaction with the constantly expanding solar atmosphere—the solar wind—and structures the plasma and charged-particle environment of the planet (*1*). By its orientation and strength, Mercury's magnetic field inhibits direct solar wind access to the planetary surface in dayside equatorial regions (*2*), where the average magnetic field orientation is nearly perpendicular to the velocity of the incoming solar wind (*3*). At high latitudes, in contrast, the solar wind interaction with the magnetic field forms northern and southern "cusps," funnel-shaped indentations in the magnetopause that capture some of the magnetosheath plasma and guide it to lower altitudes (*4*, *5*). Since Mercury lacks an appreciable atmosphere, this funneling of solar wind plasmas down to the surface is of particular importance because the incident plasma is believed to sputter neutral atoms from the surface into the exosphere and to account for a substantial portion of the exosphere's variability (*6*). Neutral exospheric particles can also be generated by other processes, such as thermal evaporation off Mercury's surface, desorption stimulated by photons or electrons, and micrometeoroid impact. Less well understood are surface processes that might lead to the direct ejection of ions from the planetary surface (*6*). Whether they originate from ionization of the neutral exosphere or from the surface, Mercury's ions subsequently undergo energization and transport by electromagnetic forces that dominate Mercury's space environment (*2*, *7*).

During its near-equatorial flybys of the innermost planet in 2008–2009, the MESSENGER spacecraft obtained initial measurements of the structure of the magnetosphere (Fig. 1). Mercury's magnetic field is highly distorted by the solar wind. On the dayside, the planetary magnetic field is compressed by the ram pressure of the incident solar wind, whereas on the nightside the magnetic field is pulled back to form a long magnetic tail (*8*). Special attention is called to the northern and southern cusp regions, from which ions from all sources stream along magnetospheric field lines into the northern and southern lobes of the tail, where they drift toward the tail's equatorial plane to concentrate and form the plasma sheet (*9*).

MESSENGER was inserted into orbit about Mercury on 18 March 2011, and here we report the results of near-continuous measurements of planetary ions near Mercury on a global scale. These measurements were made with the Fast Imaging Plasma Spectrometer (FIPS), the low-energy portion of the Energetic Particle and Plasma Spectrometer (EPPS) instrument (*10*). We focus on the spatial distribution of the most abundant ions with energy per charge *E/q* between 0.1 and 13 keV/e and with mass per charge

[1]Department of Atmospheric, Oceanic and Space Sciences, University of Michigan, Ann Arbor, MI 48109–2143, USA. [2]Heliophysics Science Division, NASA Goddard Space Flight Center, Greenbelt, MD 20771, USA. [3]The Johns Hopkins University Applied Physics Laboratory, Laurel, MD 20723, USA. [4]Laboratory for Atmospheric and Space Physics, University of Colorado, Boulder, CO 80303, USA. [5]Office of Space Research and Technology, Academy of Athens, Athens 11527, Greece. [6]Goddard Planetary Heliophysics Institute, University of Maryland, Baltimore County, Baltimore, MD 21228, USA. [7]Institute of Geophysics and Planetary Physics, University of California, Los Angeles, CA 90095, USA. [8]Department of Terrestrial Magnetism, Carnegie Institution of Washington, Washington, DC 20015, USA.

*To whom correspondence should be addressed. E-mail: thomasz@umich.edu